Estimation and Optimal Configurations for Localization Using Cooperative UAVs

Purvis, Keith B.; Åström, Karl Johan; Khammash, Mustafa

Published in:
IEEE Transactions on Control Systems Technology

2008

Estimation and Optimal Configurations for Localization Using Cooperative UAVs

Keith B. Purvis, *Member, IEEE*, Karl J. Åström, *Fellow, IEEE*, and Mustafa Khammash, *Fellow, IEEE*

***Abstract*—The time-difference of arrival techniques are adapted to locate networked enemy radars using a cooperative team of unmanned aerial vehicles. The team is engaged in deceiving the radars, which limits where they can fly and requires accurate radar positions to be known. Two time-differences of radar pulse arrivals at two vehicle pairs are used to localize one of the radars. An explicit solution for the radar position in polar coordinates is developed. The solution is first used for position estimation given "noisy" measurements, which shows that the vehicle trajectories significantly affect estimation accuracy. Analyzing the explicit solution leads to The Angle Rule, which gives the optimal vehicle configuration for the *angle* estimate. Analyzing the Fisher Information Matrix leads to The Coordinate Rule, which gives a different optimal configuration for the *position* estimate. A linearized time-varying model is also formulated and an Extended Kalman Filter applied. This estimation scheme is compared with the earlier one, with the second showing overall improvement in reducing the variance of the estimate.**

***Index Terms*—Electronic warfare, Fisher Information Matrix, Kalman filtering, localization, optimal configuration, position estimation, unmanned aerial vehicles (UAVs).**

I. Introduction

THE Estimation Problem addressed here is connected to the Cooperative Deception Problem in [1], [2]: using unmanned aerial vehicles (UAVs) to cooperatively deceive an enemy radar network by causing the network to track the motion of a phantom or nonexistent air vehicle. UAVs meeting the requirements to perform this task will be called Electronic Combat Air Vehicles (ECAVs) from here on. A radar network is defined as two or more radars that share track files to correlate a target. Methods for generating a phantom target are restricted to range-delay techniques applied through the radar main lobe. Fig. 1 illustrates the problem. For a team of ECAVs—generally one per radar—to succeed against the radar network, each ECAV's trajectory must satisfy several dynamic limitations [1]; also, the position of each radar must be accurately known.

Radar position estimation is addressed using time-differences of arrival (TDOAs). To obtain a TDOA measurement, each of two ECAVs uses a synchronized internal clock to record a time stamp on the arrival of a (unique) encoded radar pulse, and the difference between the two times is taken. One TDOA places the transmitting radar on a hyperbolic curve on the ground. Thus, based on two or more TDOAs, the radar's position can be estimated by taking the correct intersection of the hyperbolas. The estimate will not be exact due to electronic measurement noise and clock synchronization error; see [3, chap. 11] for more details on GPS-based synchronization.

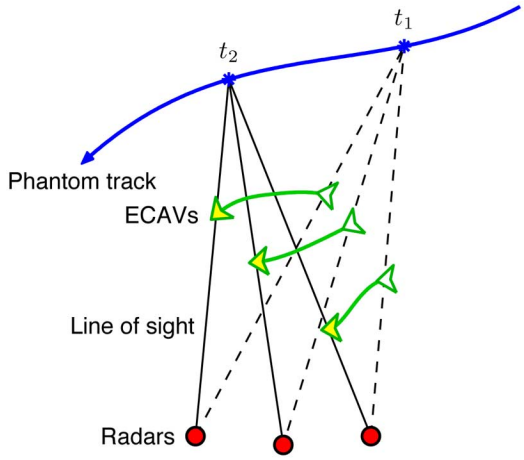

Fig. 1. Creation of a phantom radar track. Radar pulses are intercepted by a stealthy ECAV and returned with a delay so that the radar sees a phantom target beyond the ECAV. To generate a coherent phantom track for the radar network, one ECAV per radar is needed to stay on the line of sight between the radar and phantom target; the radar positions must also be known.

We proceed based on two fundamental ideas. First, the choice of ECAV trajectories flown significantly affects the accuracy of the radar position estimates. Hence, it is important to find trajectories that will minimize the variance of the estimates. Second, even the best ECAV trajectories may produce unacceptable variance; however, knowing the distribution of the measurement error allows for effective filtering. Assuming a Gaussian distribution, an Extended Kalman Filter applied to a linearized system can significantly reduce the variance of the estimates. Again, minimizing this variance through filtering and selection of optimal ECAV trajectories will improve the coherency of the generated phantom track for the radar network.

Earlier work in [4] provides the beginning for this paper, in which there are significant improvements and additions including an explicit solution for the radar position and a study of optimal vehicle configurations. A decentralized estimation scheme has also been developed for this problem [5], where vehicle constraints are communicated in terms of the phantom track and used by each vehicle to estimate the other vehicle and radar positions. However, [5] assumes that each vehicle knows

Manuscript received February 15, 2007. Manuscript received in final form November 7, 2007. First published March 31, 2008; last published July 30, 2008 (projected). Recommended by Associate Editor C. Rabbath. This work was supported in part by the National Science Foundation under Grant 0300568.

K. Purvis is with Toyon Research Corporation, Goleta, CA 93117 USA (e-mail: kpurvis@toyon.com).

K. Åström and M. Khammash are with the Department of Mechanical and Environmental Engineering, University of California, Santa Barbara, CA 93106-5070 USA (e-mail: astrom@engineering.ucsb.edu; khammash@engineering.ucsb.edu).

Color versions of one or more of the figures in this paper are available online at http://ieeexplore.ieee.org.

Digital Object Identifier 10.1109/TCST.2007.916348

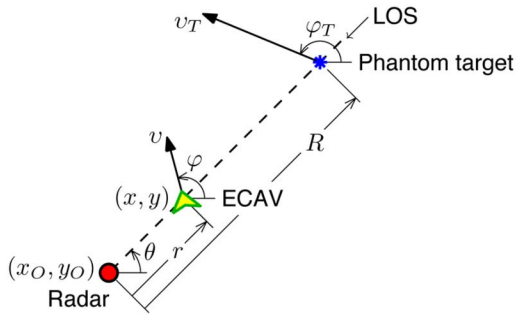

Fig. 2. ECAV and phantom track variables. The main variables are shown for one radar and ECAV, where the ECAV is on the LOS from the radar to the generated phantom target.

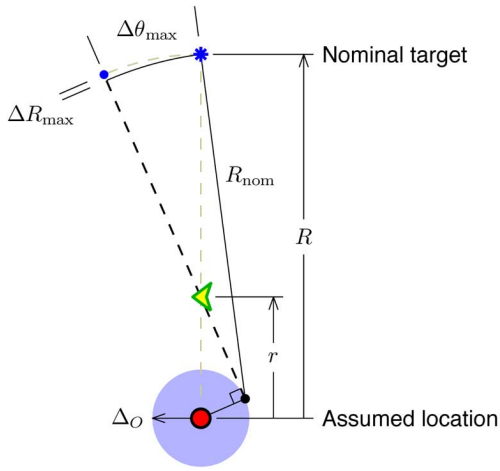

Fig. 3. Phantom variation due to an unknown radar location. The vehicle projecting the phantom target knows its position but only has an uncertainty disk for the radar defined by Δ_O centered at the assumed location. The worst case deviation in phantom range and azimuth occurs when the radar is actually located at the dot on the edge of the disk.

exactly where *its* radar is located, whereas we drop this assumption as the starting point of our study.

Our goal is to determine an estimation system and optimal vehicle configurations that will localize an emitter with minimum variance. First, we provide some background on the cooperative deception problem. An uncertainty analysis shows how inaccurate radar position estimates will lead to mission failure. Second, we lay the framework for positioning using TDOA measurements. By parametrizing the TDOA equations/hyperbolas in polar coordinates, we derive a novel, explicit solution for the radar position. This solution is used to perform estimation by direct calculation and time averaging. Third, we investigate optimal platform configurations that will minimize the error in the estimates. By analyzing our explicit solution, we get The Angle Rule, and this is compared with The Coordinate Rule via the Fisher Information Matrix. Last, we develop a linearized model for the estimation system and implement an Extended Kalman Filter; simulations are shown and compared with the earlier scheme.

II. Deception Problem Backgrounds

The scenarios considered herein are all constant-elevation since the phantom will typically fly at a constant altitude, and any minor descents can be easily decoupled and handled by the ECAVs. Assuming that an ECAV is stealthy and knows $R_{\max}$, the maximum operational range, and the location of a radar with pulse-to-pulse agility, the ECAV can intercept and send delayed returns of the radar's transmitted pulses so that the radar sees a phantom target at a range beyond the ECAV but closer than $R_{\max}$. To maintain deception, each ECAV behaves much like a bead on a string that is rotating at some variable rate; the ECAV may slide up or down freely but must rotate with the line of sight (LOS) from the radar to the phantom track. In other words, the ECAV has one constraint, $\theta(t)$, and one degree of freedom over time. Fig. 2 shows the main variables and their relations.

The phantom track is assumed given since there are already many criteria besides accurate position estimation governing its selection [6]. Without loss of generality, $\dot{\theta}$ is also assumed positive. We use a constant-heading, constant-speed phantom track only for simplicity, which is given by

$$R(t) = \sqrt{R_0^2 + v_T^2 t^2 + 2R_0 v_T t \cos\phi_{T0}}$$

$$\theta(t) = \arcsin\left[\frac{v_T t \sin\phi_{T0}}{R(t)}\right] + \theta_0$$

$$\dot{\theta}(t) = \frac{R_0 v_T \sin\phi_{T0}}{R^2(t)}$$

where $\phi_T := \varphi_T - \theta$ (see Fig. 2 for most of the variables used). The subscript 0 refers to when $t = 0$. To generate the phantom track, each ECAV flies a bearing of $\theta_i(t)$ from its radar and uses range-delay techniques as previously described to put a phantom target at the range $R_i(t)$, where i indexes the ECAVs.

For this work, we put our ECAV model in the Cartesian frame:

$$\begin{aligned} \dot{x} &= v\cos\varphi, \quad x(0) = x_0 \\ \dot{y} &= v\sin\varphi, \quad y(0) = y_0 \\ \dot{\varphi} &= u, \quad \varphi(0) = \varphi_0 \end{aligned} \tag{1}$$

$$v = \frac{\dot{\theta}\sqrt{x^2 + y^2}}{\sin(\varphi - \theta)} \tag{2}$$

where the control u is the vehicle heading rate. The reason for using Cartesian instead of polar coordinates is that with the position of the radar unknown, the coordinates (r, θ) would have an unknown origin. Based on the ECAV dynamics, u is restricted to be piecewise continuous. Since $\dot{\theta}$ is positive, $\theta(t) < \varphi < \theta(t) + \pi$ is also required. To remain in sync with the phantom track, the ECAV must constantly adjust its speed as given by (2).

A. Uncertainty Analysis

Since the main reason for estimating the radar positions is to maintain a coherent phantom track for the radar network, it is essential to examine just how much the phantom target is affected by an assumed radar location that is inaccurate. This inaccuracy contributes to a region of uncertainty around a nominal phantom target where the target may actually be placed by an unsuspecting ECAV. If the region is too large, then the networked radars will be able to discriminate between their respectively observed phantom targets and "see" through the deception. Given an uncertainty in the radar location of Δ_O, Fig. 3

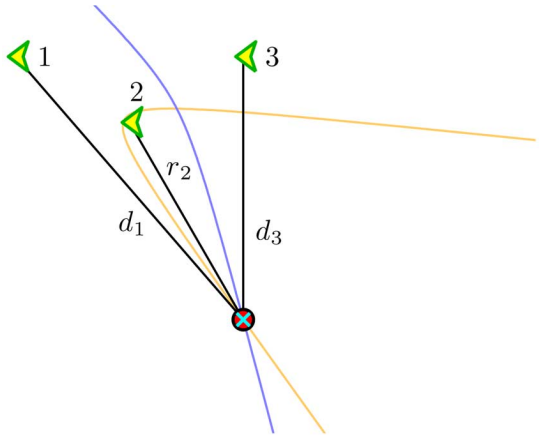

Fig. 4. Estimation of the middle radar position without noise. Three vehicles/sensors can localize a radar/emitter using two TDOA measurements. Without noise, $n_1, n_2 = 0$, the estimate is exact.

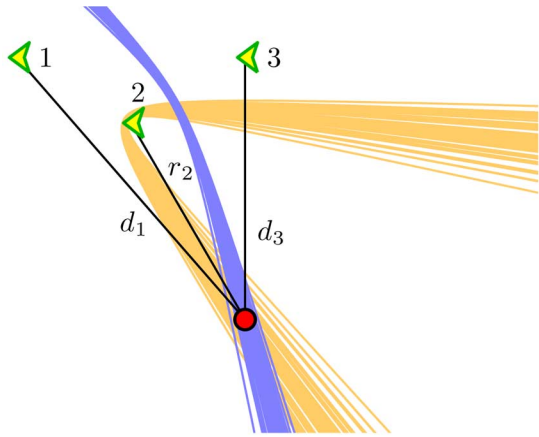

Fig. 5. Hyperbolic bands resulting from measurement noise. White noise entering the TDOA measurements, $n_1, n_2 \neq 0$, causes a spread of hyperbolic bands, which do not exactly touch the unknown radar location. Thus, the vehicles seeking to localize the radar will get an inexact estimate.

shows the worst case situation that would produce maximum deviation in both the range and bearing/azimuth of the phantom target. Using the figure as a guide, we get the following equations:

$$\Delta R_{\max} = \sqrt{r^2 - \Delta_O^2} + (R - r) - R_{\text{nom}} \tag{3}$$

$$\Delta\theta_{\max} = \arcsin\left[\frac{\Delta_O/r}{R_{\text{nom}}}(R - r)\right]$$

$$R_{\text{nom}} = \sqrt{R^2 + \Delta_O^2(1 - 2R/r)}. \tag{4}$$

With $R = 30$ km and $r = 5$ km, the critical radar resolutions for $\Delta_O = 100$ m are $\Delta R_{\max} = 0.833$ m in range and $2(\Delta\theta_{\max}) = 1.91°$ in azimuth. The critical resolution for azimuth is double that of (4) since one ECAV could be projecting $+\Delta\theta_{\max}$ and another $-\Delta\theta_{\max}$; however, $\Delta R_{\max}$ can only be positive. If the radars were to have a resolution better/smaller than the calculated resolutions, then the phantom track would be dismissed as spurious. We observe that the critical range resolution is so small as to be inconsequential; indeed, the type of aircraft desirable for the phantom to emulate would be on the order of tens of meters. However, the critical azimuth resolution is significant; to get a better idea, convert to distance at the range $R = 30$ km, which gives 1 km for 1.91°. Thus, knowing the radar location accurately in terms of angle is important, whereas range is not.

In summary, the phantom track deception can be successful *if* the radar locations or angles are known. Otherwise, each ECAV's expected placement of the phantom target may be significantly different from its actual placement, which will result in an incoherent phantom track for the radar network. Therefore, we proceed to find methods to accurately estimate the radar positions.

III. Radar Positioning Using Time Differences

We assume for now that the ECAVs know their exact positions. We also assume that the ECAVs have synchronized clocks and can detect pulses from radar side lobes, which are much weaker in power than those from the main lobe. The side-lobe assumption is necessary for the ECAVs to obtain TDOA measurements of radar pulses since each radar looks directly at only one of the ECAVs. Side lobes are normally actively suppressed to attenuate noise leaking in from nearby sources or reflectors, so as to maximize the signal-to-noise ratio for the signal from the main-lobe direction. However, side lobes cannot be entirely eliminated, and it is much easier to receive side lobe transmissions than it is to detect their (reflected) return ($\sim 1/r^2$ versus $1/r^4$). To simplify analysis, just the position of the middle radar—that corresponding to ECAV 2—is estimated using two TDOA measurements[1] from ECAV pairs 1–2 and 3–2. The measurements—converted to distance—are modeled by

$$\begin{aligned}\Delta_1 &:= c_l(\tau_1 - \tau_2) = d_1 - r_2 + n_1\\ \Delta_2 &:= c_l(\tau_3 - \tau_2) = d_3 - r_2 + n_2\end{aligned} \tag{5}$$

where c_l is the speed of light, τ_i is the measured pulse arrival time at the ith ECAV, and n_1 and n_2 are the combined noise/error from the arrival times. The other variables are shown in Fig. 4, which illustrates the ideal case when two noise-free measurements $(n_1, n_2 = 0)$ are used to determine the position of the middle radar. Since Δ_1 and Δ_2 are distance differences, they naturally give rise to hyperbolas, on which the emitting radar must be located. With white noise added $(n_1, n_2 \neq 0)$ to approximate the collective effect of electronic measurement noise and clock synchronization error[2] in the τ_i's, hyperbolic bands are created as shown in Fig. 5. Intuitively, the variance of the position estimates will be smaller when the ECAVs are more spread apart in angle.

Note that only Δ_1 and Δ_2 can be measured—absolute distances and pulse travel times are unknown. Obtaining a Δ given streams of pulse arrival times from two ECAVs requires communication and some signal processing to match up the two profiles by their corresponding encoded radar pulses. With only

[1]If more than two measurements are used, then the system of equations is overdetermined, and methods such as nonlinear least squares as in [7] or Kalman filtering may be used to find the best "average" position estimate.

[2]A first-order Gauss-Markov process would be more accurate for GPS synchronization according to [3, Ch. 11], but a Gaussian random process is used for simplicity.

two TDOAs/hyperbolas, more than one intersection will result in most cases. One of the two halves of each hyperbola can be ruled out based on the signs of Δ_1 and Δ_2 (as done in Fig. 4), which leaves two intersections in general. However, the correct intersection nearest the true position of the middle radar can be identified by discriminating the intersections as the ECAVs move over time, or by assuming an approximate location for the radar is previously known.

There are other methods for locating emitters besides using TDOA measurements, which include angle of arrival (AOA), received signal strength (RSS), and time of arrival (TOA) or travel time (see [8] for more details). However, using AOA measurements would be less accurate than TDOA, especially given an inexpensive antenna likely for an ECAV. RSS assumes that the transmitted power is known so that its attenuation over distance can be computed and compared with the actual received signal, but the transmitted power is unknown in our case, and a radar can modulate its transmitted power in normal operation. TOA introduces a clock bias parameter and cannot be used in our case because the time at which a pulse leaves the radar is unknown, hence travel time cannot be determined.

IV. Explicit Solution for the Radar Position

Calculating the exact intersection of two hyperbolas is difficult, and many efforts have been made to do so as outlined in [9]. Here, we give an alternative solution not found in [9], which is particularly useful for our case due to the polar parametrization. First, parametrize each hyperbola in polar coordinates (ρ, β) with the middle vehicle as the common origin

$$\rho_{h1}(\beta) = \frac{\frac{1}{2}\left(r_{12}^2 - \Delta_1^2\right)}{\Delta_1 + r_{12}\cos(\beta - \theta_{12})} \tag{6}$$

$$\rho_{h2}(\beta) = \frac{\frac{1}{2}\left(r_{32}^2 - \Delta_2^2\right)}{\Delta_2 + r_{32}\cos(\beta - \theta_{32})} \tag{7}$$

where r_{i2} and θ_{i2} are the range and bearing, respectively, of ECAV i from ECAV 2. The reason we choose ECAV 2 as the origin for the coordinates is that it is the vehicle assigned to deceive the middle radar, and radar position estimates should be relative to the ECAV using them. As designated, the functions $\rho_{h1}(\beta)$ and $\rho_{h2}(\beta)$ do map each angle β to a unique range ρ even though from a plot like Fig. 4, it might appear that using ECAV 2 as the origin gives two ranges for some values of β. However, one must realize that the point (ρ, β) can also be represented by $(-\rho, \beta + \pi)$. The emitting radar must be located on the half of the hyperbola having positive values for ρ.

To form a hyperbola requires that the eccentricity $r_{i2}/|\Delta|$ be greater than one, where Δ appears with r_{i2} in either (6) or (7). This gives rise to an important condition for the measurements:

$$r_{i2} > |\Delta|. \tag{8}$$

If the measurement Δ has zero noise, then condition (8) will always be met, modulo equality when both vehicles in the pair have the same bearing from the radar (this gives a parabola). If the noise is nonzero, then (8) may be violated as $r_{i2} < |\Delta|$, which results in an ellipse instead of a hyperbola. Violation becomes more likely when r_{i2} is small or both vehicles have similar bearings.

Equating (6) and (7) gives a trigonometric equation, which has two solutions for β and hence for position

$$\hat{\beta} = \arcsin\frac{-c}{\sqrt{a^2 + b^2}} - \operatorname{arccot}\frac{b}{a} \tag{9}$$

$$\hat{\rho} = \rho_{h1}(\hat{\beta}) = \rho_{h2}(\hat{\beta}) \tag{10}$$

$$a = r_{32}\cos\theta_{32}\left(r_{12}^2 - \Delta_1^2\right) - r_{12}\cos\theta_{12}\left(r_{32}^2 - \Delta_2^2\right)$$

$$b = r_{32}\sin\theta_{32}\left(r_{12}^2 - \Delta_1^2\right) - r_{12}\sin\theta_{12}\left(r_{32}^2 - \Delta_2^2\right)$$

$$c = \Delta_2\left(r_{12}^2 - \Delta_1^2\right) - \Delta_1\left(r_{32}^2 - \Delta_2^2\right).$$

With zero noise, it can be shown that $a > 0$ provided that none of the ECAVs share the same bearing from the middle radar. The two solutions for $\hat{\beta}$ come from taking the $\arcsin$, and this angle is always in the first quadrant for the scenarios we work with. The corresponding range $\hat{\rho}$ can be found by substituting $\hat{\beta}$ into (6) or (7) as shown by (10). For ECAV 2 to compute $\hat{\beta}$, it needs the relative ranges and angles of the other ECAVs providing measurements. If there is no noise in the measurements Δ_1 and Δ_2, then the position estimate $(\hat{\rho}, \hat{\beta})$ is exact. With noise, the estimate is only approximate.

This solution is well-suited to our application and different from the many solutions in [9] because the angle of the position estimate can be directly calculated and analyzed without first obtaining $(\hat{x}_O, \hat{y}_O)$ or $\hat{\rho}$, which are not really needed. Specifically, for an ECAV generating a phantom track using range-delay techniques, the distance r from the ECAV to the radar is not important, but rather the distance from the ECAV to the phantom, $(R - r)$. As long as the latter is known, which would be true with the ECAV position and phantom track known, the ECAV can intercept and appropriately delay radar pulses by the delay time $2(R - r)/c_l$, where c_l is the speed of light. Coupled with an accurate angle estimate $\hat{\beta}$, this allows the ECAV to place a phantom target where intended without knowing how far away the radar is (see also Fig. 3 and accompanying discussion). The range estimate is still useful in secondary ways and for other problems, so it should not be disregarded entirely. It is also used here to convert to $(\hat{x}_O, \hat{y}_O)$ for measuring the performance of the estimation schemes.

A. Simulations of Estimation by Direct Calculation

We now apply the results from Section IV to estimate the middle radar position over time in a scenario with a fixed phantom track. The measurement noise is Gaussian with intensity 0.0001 km^2/Hz for both measurements, which corresponds to a 1σ-error of 30 m with a measurement taken every 0.1 s. Instead of assuming that there is no temporal correlation of the position, we capitalize on the stationarity of the radar and take a running average of the estimates over time. This strategy is effective as long as the distribution of the estimates is approximately normal. In this and subsequent simulations, the performance of the estimation scheme is measured by the root mean square error (RMSE), which is defined for Cartesian coordinates as

$$\text{RMSE}_{xy} = \sqrt{\text{E}[(x_O - \hat{x}_O)^2 + (y_O - \hat{y}_O)^2]} \tag{11}$$

where x_O and y_O are the true coordinates of the middle radar, and $\hat{x}_O$ and $\hat{y}_O$ are the corresponding estimates, all relative to

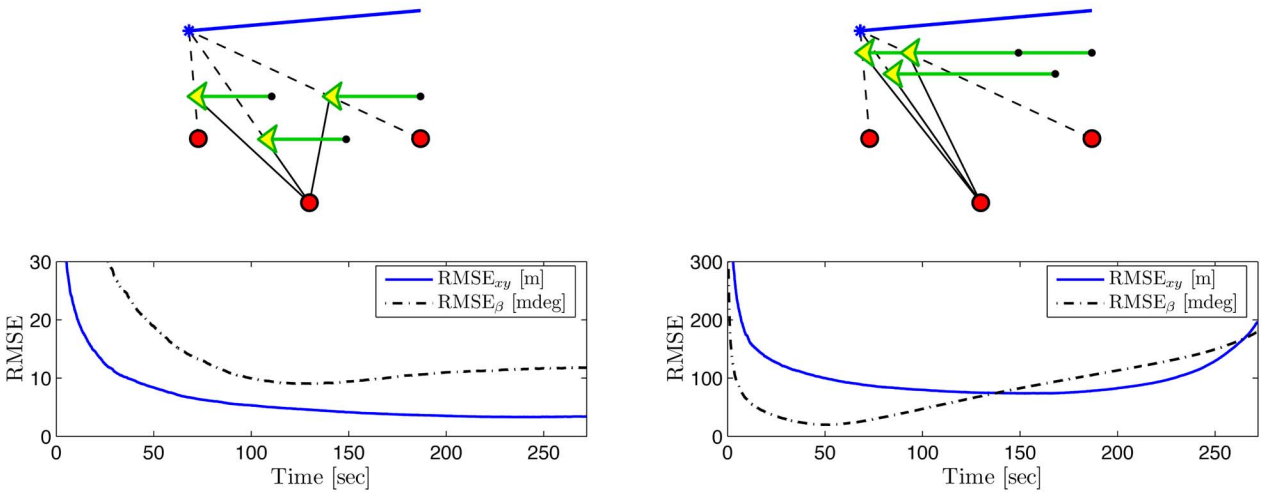

(a) for $\frac{r_0}{R_0} = 0.33$ (b) for $\frac{r_0}{R_0} = 0.67$

Fig. 6. Estimation of the middle radar position using the explicit solution. The radar position is directly calculated and the estimates averaged over time; the measurement noise has intensity 0.0001 km^2/Hz, and 1000 runs are made. The root mean square errors of the position and angle estimates are plotted as RMSE$_{xy}$ and RMSE$_{\beta}$, respectively. The only difference between the two scenarios is how far the vehicles are from the radars, which affects their relative separation angles and hence the errors.

some fixed reference frame. We also use the RMSE for the angle estimate, which is

$$\text{RMSE}_{\beta} = \sqrt{\text{E}[(\beta - \hat{\beta})^2]} \tag{12}$$

where β is the angle of the middle radar, and $\hat{\beta}$ is the corresponding estimate, all relative to a polar frame with the middle vehicle as the origin. The expectation is taken over 1000 runs unless otherwise stated.

Fig. 6 shows two scenarios where position estimation is done by direct calculation using (9)–(10) and time averaging. The phantom track is straight with a constant speed of 100 m/s and a length of approximately 26 km. The only difference between the two scenarios is the ECAV trajectories, which are governed by (1)–(2). Both the RMSE$_{xy}$ and the RMSE$_{\beta}$ are plotted for each scenario. For each run, the measurement noise sequences are chosen randomly.

Observing Fig. 6(a), halfway through the time interval the RMSE$_{xy}$ decreases to roughly 5 m and tends to level off as time increases. In Fig. 6(b), the RMSE$_{xy}$ decreases to roughly 100 m and then starts increasing sharply as time increases. The key difference between the two scenarios, and what causes the RMSE to increase with time in the second scenario, is not how far the ECAVs are from the radars but how spread apart in angle; we will substantiate this idea in the next section. Fig. 6 also shows that in the transient, the RMSE$_{\beta}$ does not track the RMSE$_{xy}$, although obviously $\lim_{t\to\infty} \text{RMSE}_{xy} = 0 \Rightarrow \lim_{t\to\infty} \text{RMSE}_{\beta} = 0$ (the other direction does not hold).

V. Optimal Vehicle Configurations

Fig. 6 suggests that the estimation error is lower when the vehicles are sufficiently spread apart in angle, and we formally pursue this idea. The explicit solution from Section IV is used to determine vehicle configurations that minimize the sensitivity of the estimate $\hat{\beta}$ to measurement noise, and this gives The Angle Rule. The Fisher Information Matrix also gives an additional perspective, and by it we get The Coordinate Rule. Combined together, these results provide an understanding for how the optimal configurations depend on the form of the estimate one is concerned with.

A. Angle Rule (Using the Explicit Solution)

Before finding the sensitivity of $\hat{\beta}$ to measurement noise, some new variables are introduced: the relative distance $\alpha_i := d_i/r_2$ and the separation angle $\bar{\theta}_i := |\theta_{iO} - \theta_{2O}| \in [0, 2\pi]$, where $\theta_{1O} \geq \theta_{2O} \geq \theta_{3O}, \bar{\theta}_1 + \bar{\theta}_3 \leq 2\pi$, and $\theta_{2O} = 90^\circ$ to orient the geometry. Please see Fig. 7 in this section.

We now use (9) to calculate the sensitivities $(\partial\hat{\beta}/\partial n_1)$ and $(\partial\hat{\beta}/\partial n_2)$, where n_1 and n_2 are the noises that enter the measurements (5). The partial derivative is first written as

$$\frac{\partial\hat{\beta}}{\partial n} = \frac{\partial\hat{\beta}}{\partial\Delta}\frac{\partial\Delta}{\partial n} = \frac{\frac{c}{a^2+b^2}\left(a\frac{\partial a}{\partial\Delta} + b\frac{\partial b}{\partial\Delta}\right) - \frac{\partial c}{\partial\Delta}}{\sqrt{a^2+b^2-c^2}} + \frac{a\frac{\partial b}{\partial\Delta} - b\frac{\partial a}{\partial\Delta}}{a^2+b^2} \tag{13}$$

where n is a generic noise, and a, b, and c are given in (9)–(10). Since we are interested in noise with zero mean, each term must be evaluated at $n_1, n_2 = 0$. It can be shown that $b|_{n_1,n_2=0} = c|_{n_1,n_2=0}$, and this allows us to simplify (13) to

$$\left.\frac{\partial\hat{\beta}}{\partial n}\right|_{n_1,n_2=0} = \frac{1}{a|_{n_1,n_2=0}}\left(\left.\frac{\partial b}{\partial\Delta}\right|_{n_1,n_2=0} - \left.\frac{\partial c}{\partial\Delta}\right|_{n_1,n_2=0}\right). \tag{14}$$

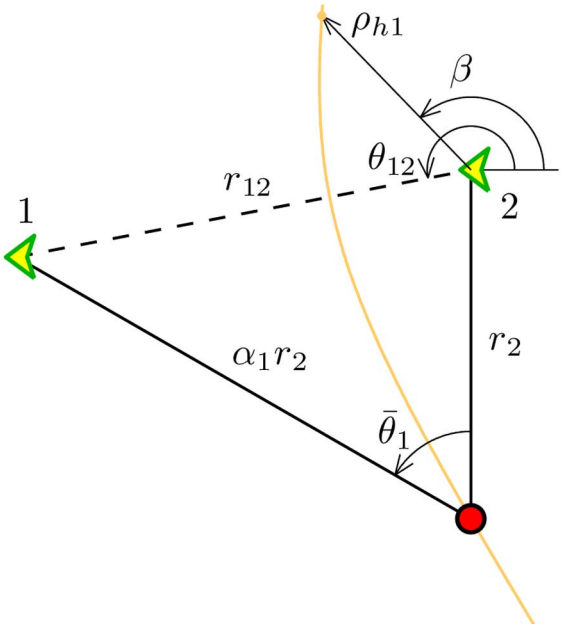

Fig. 7. Angle analysis variables. The relevant variables for working with the hyperbolas are shown, which are used to determine the sensitivity of the angle estimate to measurement noise.

The remaining terms are calculated for both Δ_1 and Δ_2 by using (5), converting to the variables $(r_2, \alpha_i, \bar{\theta}_i)$, and evaluating at zero noise, which gives

$$\begin{aligned}
a|_{n_1,n_2=0} &= 2r_2^3\alpha_1\alpha_3[\sin\bar{\theta}_3(1-\cos\bar{\theta}_1) \\
&\quad + \sin\bar{\theta}_1(1-\cos\bar{\theta}_3)] \\
\left.\frac{\partial b}{\partial \Delta_1}\right|_{n_1,n_2=0} &= 2r_2^2(\alpha_1-1)(1-\alpha_3\cos\bar{\theta}_3) \\
\left.\frac{\partial b}{\partial \Delta_2}\right|_{n_1,n_2=0} &= -2r_2^2(\alpha_3-1)(1-\alpha_1\cos\bar{\theta}_1) \\
\left.\frac{\partial c}{\partial \Delta_1}\right|_{n_1,n_2=0} &= -2r_2^2[(\alpha_1-1)(\alpha_3-1)+\alpha_3(1-\cos\bar{\theta}_3)] \\
\left.\frac{\partial c}{\partial \Delta_2}\right|_{n_1,n_2=0} &= 2r_2^2[(\alpha_1-1)(\alpha_3-1)+\alpha_1(1-\cos\bar{\theta}_1)].
\end{aligned}$$

Finally, these terms are inserted into (14) to get the sensitivities

$$\left.\frac{\partial\hat{\beta}}{\partial n_1}\right|_{n_1,n_2=0} = \frac{1}{r_2}\frac{(1-\cos\bar{\theta}_3)}{\sin\bar{\theta}_1+\sin\bar{\theta}_3-\sin(\bar{\theta}_1+\bar{\theta}_3)} \quad (15)$$

$$\left.\frac{\partial\hat{\beta}}{\partial n_2}\right|_{n_1,n_2=0} = \frac{1}{r_2}\frac{-(1-\cos\bar{\theta}_1)}{\sin\bar{\theta}_1+\sin\bar{\theta}_3-\sin(\bar{\theta}_1+\bar{\theta}_3)} \quad (16)$$

Based on (15) and (16), we observe that the distances of the outer vehicles, ECAVs 1 and 3, do not affect the (first-order) sensitivity of the estimate to measurement noise. While r_2 does affect the sensitivity of $\hat{\beta}$ in both (15) and (16), one should view this only as a conversion from distance (in the x direction in this case) to angle, i.e.,

$$\frac{\partial\hat{\beta}}{\partial n} = \frac{1}{r_2}\frac{\partial\hat{x}_O}{\partial n}$$

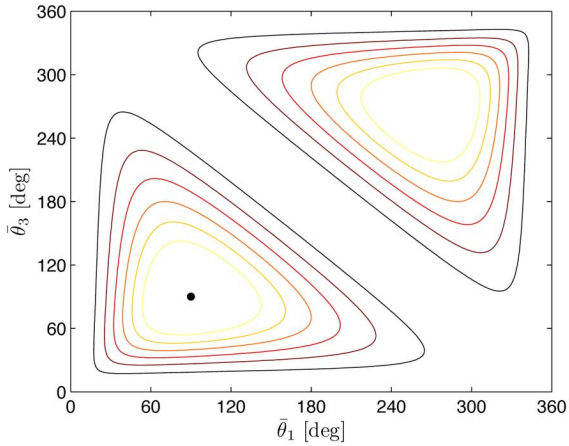

Fig. 8. Level curves of the information function $J_\beta(\bar{\theta}_1, \bar{\theta}_3)$. Given that $\bar{\theta}_1 + \bar{\theta}_3 \leq 2\pi$, J_β has a unique maximum at $\bar{\theta}_1 = 90^\circ, \bar{\theta}_3 = 90^\circ$ (denoted by the large dot), which is The Angle Rule.

for $\theta_{2O} = 90^\circ$.

The two sensitivities (15) and (16) must somehow be combined to obtain the overall worst case sensitivity of $\hat{\beta}$ to measurement noise. Comparing the numerators of both shows that n_1 and n_2 influence $\hat{\beta}$ in opposite directions. Since $(1-\cos\bar{\theta}_i)$ is nonnegative, subtracting the two sensitivities will always yield a magnitude greater than or equal to that gotten by adding. That is, for any given angles $\bar{\theta}_1$ and $\bar{\theta}_3$, $\hat{\beta}$ will be more sensitive when the measurement noises n_1 and n_2 have opposite signs. Therefore, we seek to minimize the magnitude of $((\partial\hat{\beta}/\partial n_1)-(\partial\hat{\beta}/\partial n_2))$ or maximize its inverse squared, which we call $J_\beta : (0,2\pi)\times(0,2\pi) \to \mathbb{R}_+ \cup \{0\}$ and present

$$\begin{aligned}
J_\beta(\bar{\theta}_1,\bar{\theta}_3) &:= \frac{1}{\left(\left.\frac{\partial\hat{\beta}}{\partial n_1}\right|_{n_1,n_2=0} - \left.\frac{\partial\hat{\beta}}{\partial n_2}\right|_{n_1,n_2=0}\right)^2} \\
&= \left(\frac{\sin\bar{\theta}_1+\sin\bar{\theta}_3-\sin(\bar{\theta}_1+\bar{\theta}_3)}{2-\cos\bar{\theta}_1-\cos\bar{\theta}_3}\right)^2 \quad (17)
\end{aligned}$$

In keeping with the domain, direction, and ordering for $\bar{\theta}_1$ and $\bar{\theta}_3$, the information function J_β has a unique maximum at $\bar{\theta}_1 = \bar{\theta}_3 = 90^\circ$ (see Fig. 8). If both angles are assumed equal, then (17) reduces to

$$J_\beta(\bar{\theta},\bar{\theta}) = \sin^2\bar{\theta}$$

which is a simple way to remember how the separation angles affect the sensitivity of the angle estimate to measurement noise, with larger values of J_β reflecting lower sensitivity or better information. Thus, J_β tells us that to maximize the accuracy of the angle estimate $\hat{\beta}$, the separation between ECAVs 1 and 2 and ECAVs 2 and 3 should be 90°; we call this *The Angle Rule*. While the distances of the ECAVs from the middle radar do not affect the first-order sensitivity of $\hat{\beta}$, they do have higher-order effects, but we do not pursue this topic here.

To compute an explicit intersection using (9), and (10), one needs exactly two hyperbolas/TDOAs, which requires three vehicles. However, pulse arrival times from three vehicles give rise to *three* hyperbolas; two of these must be chosen, which in our

case is equivalent to choosing the common origin for the polar coordinates (ρ, β). We can use (17) to show that, for a given configuration with separation angles $\bar{\theta}_1, \bar{\theta}_3 \leq 90°$, the middle vehicle or ECAV 2 is the best to use as the common origin. We begin with $\bar{\theta}_1$ and $\bar{\theta}_3$, which were defined with ECAV 2 as the origin (see Fig. 7), and redefine them so that ECAV 1 is the new origin

$$\bar{\theta}_1' = 2\pi - (\bar{\theta}_1 + \bar{\theta}_3)$$
$$\bar{\theta}_3' = \bar{\theta}_1.$$

Substituting $\bar{\theta}_1'$ and $\bar{\theta}_3'$ into (17) and using the angle sum and difference identities, we get the following:

$$J_\beta(\bar{\theta}_1', \bar{\theta}_3') = \left(\frac{\sin\bar{\theta}_1 + \sin\bar{\theta}_3 - \sin(\bar{\theta}_1 + \bar{\theta}_3)}{2 - \cos\bar{\theta}_1 - \cos(\bar{\theta}_1 + \bar{\theta}_3)} \right)^2. \quad (18)$$

The function here is identical to the original except for the term $\cos\bar{\theta}_3$ in (17), which becomes $\cos(\bar{\theta}_1 + \bar{\theta}_3)$ in (18). By the assumption $\bar{\theta}_1, \bar{\theta}_3 \in (0, \pi/2)$, we have $0 < \bar{\theta}_1 + \bar{\theta}_3 < \pi$, and hence on this interval

$$\bar{\theta}_3 < \bar{\theta}_1 + \bar{\theta}_3 \Rightarrow \cos\bar{\theta}_3 > \cos(\bar{\theta}_1 + \bar{\theta}_3)$$
$$\Rightarrow J_\beta(\bar{\theta}_1, \bar{\theta}_3) > J_\beta(\bar{\theta}_1', \bar{\theta}_3')$$

which shows that the information gain will always be higher or the sensitivity to noise lower when the "middle" vehicle—the one with both separation angles less than 90°—is used as the origin.

Given the constraints $\theta_i(t)$ imposed by the phantom track on the ECAVs, (17) may also be used as a cost function—pointwise or integral—to determine ECAV trajectories that minimize the estimation error due to measurement noise. In addition to the vehicle configuration, J_β also depends on the unknown radar position (x_O, y_O), and there are several options to deal with this dependency (we rewrite J_β as $\bar{J}_\beta$ to include these additional variables)

$$J_1 = \bar{J}_\beta(\hat{x}_O, \hat{y}_O, \bar{\theta}_1, \bar{\theta}_3)$$
$$J_2 = \mathrm{E}_{(x_O, y_O)}[\bar{J}_\beta(x_O, y_O, \bar{\theta}_1, \bar{\theta}_3)]$$
$$J_3 = \min_{x_O, y_O} \bar{J}_\beta(x_O, y_O, \bar{\theta}_1, \bar{\theta}_3).$$

In J_1, the current estimate is used in $\bar{J}_\beta$ at each step, which makes the cost dynamic based on how the estimate is evolving. In J_2, an expectation is taken with respect to a (possibly time-dependent) probability density function for (x_O, y_O). In J_3, the minimum is taken over all "possible" radar locations. The first option is preferred in general because it adapts to changes in the estimate. However, the second or third option may be helpful at first if the initial estimate is poor. Using any of these costs, we can find ECAV controls u_1, u_2, and u_3 that yield optimal trajectories through (1)–(2).

Additional dynamic constraints on the ECAVs and phantom make it difficult to simply employ J_β in a guidance law [1]. These constraints form the coupled cooperative problem treated in [10], which provides an extensive framework for maintaining feasibility that would allow inserting J_β for choosing the optimal ECAV heading at each step. There are also motion coordination algorithms that could be adapted to steer the ECAVs using The Angle Rule [11]. Note that if all three radars were being localized, then three cost functions—one for each radar—would need to be optimized together.

The function J_β in (17) is an analogue of the Fisher Information Matrix because it quantifies the sensitivity of the estimate due to stochastic variability in the measurements, or the information gain for a given sensor configuration ($\bar{\theta}_1, \bar{\theta}_3$ in our case). A larger value of J_β indicates more information or a less sensitive estimate. More will be said about this in the next section.

B. Coordinate Rule (What the Fisher Information Gives)

For a nonrandom parameter vector q, the Cramér–Rao lower bound (CRLB) states that the covariance matrix of an unbiased estimator[3] is bounded from below[4] as

$$\mathrm{cov}\hat{q} \geq M^{-1} \quad (19)$$

where the Fisher Information Matrix (FIM) is

$$M := -\mathrm{E}[\nabla_q^2 \ln\Lambda(q)]|_{q=q_0}$$
$$= \mathrm{E}[(\nabla_q \ln\Lambda(q))(\nabla_q \ln\Lambda(q))^{\mathrm{T}}]|_{q=q_0}$$

with q_0 the true value (see [12] for theory). Assuming that a vector of uncorrelated normally distributed measurements z—with mean μ and covariance R—is being used for estimation, the likelihood function of q is

$$\Lambda(q) := p(z|q)$$
$$= \frac{1}{\sqrt{(2\pi)^{n_q} \det R}} e^{-\frac{1}{2}(z-\mu)^{\mathrm{T}} R^{-1}(z-\mu)}.$$

The FIM quantifies the total amount of information in the measurements about q. An efficient estimator, then, is one that extracts all the information or achieves equality of (19). With our measurement model (25) and some simple calculations, we have

$$M = (\nabla_q h)_{q_0}^{\mathrm{T}} R_e^{-1} (\nabla_q h)_{q_0}$$

where q is the radar position and $h = [h_1(q,t)\ h_2(q,t)]^{\mathrm{T}}$ at a given t (see (25) for the definitions of h and R_e); note that h also depends on the vehicle configuration. Finally, since $\nabla_q h$ is just the measurement matrix C for a linearized version of the system, the FIM can be written as

$$M = C^{\mathrm{T}} R_e^{-1} C. \quad (20)$$

We want to stress that M is the FIM given the measurements z at an instant of time; if all the measurements from $t = 0$ to the current time were used, then (20) would need to be integrated over this interval.

We seek a metric that will allow us to determine vehicle configurations that make M "large" and so minimize the CRLB,

[3]An estimator is unbiased if the estimation error has zero mean.

[4]Here, by $A_1 \geq A_2$ we mean $A_1 - A_2$ is positive semidefinite.

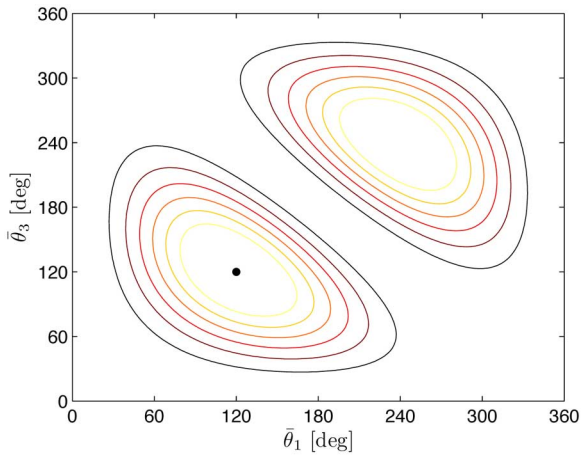

Fig. 9. Level curves of the information function $J_{xy}(\bar{\theta}_1, \bar{\theta}_3)$. Given that $\bar{\theta}_1 + \bar{\theta}_3 \leq 2\pi$, J_{xy} has a unique maximum at $\bar{\theta}_1 = 120°, \bar{\theta}_3 = 120°$ (denoted by the large dot), which is The Coordinate Rule.

which by (19) will guarantee better performance[5] on average. A suitable criterion is $\det M$ with $R_e = I$, which is similar to the "D-optimum design" found in [13] and minimizes the area of the uncertainty ellipse for the coordinate estimates. Using (29) for C, which is based on Cartesian coordinates for the radar position, and inserting this into (20), the function can be written as

$$J_{xy}(\bar{\theta}_1, \bar{\theta}_3) := \det(C^{\mathrm{T}}C) = [\sin\bar{\theta}_1 + \sin\bar{\theta}_3 - \sin(\bar{\theta}_1 + \bar{\theta}_3)]^2 \quad (21)$$

where we have again converted from absolute angles to the positive separation angles $\bar{\theta}_1, \bar{\theta}_3$, which share θ_{2O} as their zero reference (see Fig. 7). Notice the similarity between (21) and (17). In keeping with the domain, direction, and ordering for $\bar{\theta}_1$ and $\bar{\theta}_3$, the information function J_{xy} has a unique maximum at $\bar{\theta}_1 = \bar{\theta}_3 = 120°$ (see Fig. 9). Thus, J_{xy} tells us that to maximize the accuracy of the position estimate $(\hat{x}_O, \hat{y}_O)$, the separation between ECAVs 1 and 2 and ECAVs 2 and 3 should be 120°; we call this *The Coordinate Rule*.

Comparing the results in Figs. 8 and 9, one might think that there is a conflict. However, J_β reflects the information gain for the *angle* of the estimate whereas J_{xy} is for the *coordinates* of the estimate. In other words, the optimal separation angles based on J_β will maximize the accuracy of the angle estimate, and the optimal separation angles based on J_{xy} will maximize the accuracy of the position estimate. Table I sums up these two important conclusions, which are The Angle Rule and The Coordinate Rule, respectively. The shaded areas in the table represent the shape of the estimation errors being minimized.

Using the two vehicle configurations from Table I and an Extended Kalman Filter to update the measurement matrix with the current estimate,[6] we get simulations—shown in Fig. 10—that

[5]This guarantee only holds for a static estimation scenario or when the radar is stationary; for dynamic scenarios, better performance is also anticipated as shown by simulations in [11].

[6]See Sections VI and VII for the model and estimation theory used here.

TABLE I
OPTIMAL CONFIGURATIONS FOR ESTIMATION ACCURACY

The Angle Rule	The Coordinate Rule
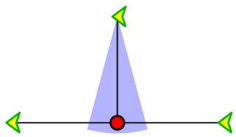	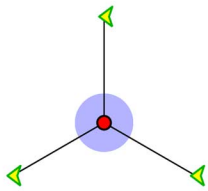
$\bar{\theta}_1 = 90°$ $\bar{\theta}_3 = 90°$	$\bar{\theta}_1 = 120°$ $\bar{\theta}_3 = 120°$

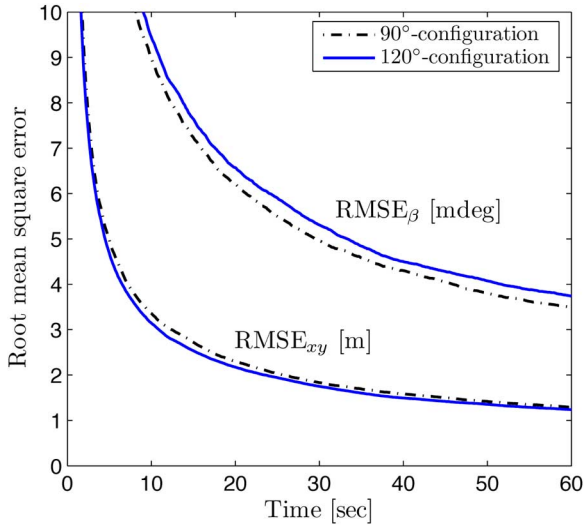

Fig. 10. Estimation with both configurations in Table I. Static vehicle configurations following The Angle Rule and The Coordinate Rule are both used with an Extended Kalman Filter to estimate the position of the middle radar (4000 runs). As predicted, the 90°-configuration yields lower error for the angle estimate (RMSE$_\beta$), and the 120°-configuration yields lower error for the position estimate (RMSE$_{xy}$).

agree with our theoretical results. The measurement noise has intensity 0.0001 km^2/Hz, and 4000 runs are made. The errors for both the coordinate and the angle estimates are plotted and measured using (11) and (12), respectively. The solid lines correspond to using The Angle Rule and the dashed to using The Coordinate Rule. Observing Fig. 10, the 120°-configuration does better in terms of position accuracy, but the 90°-configuration outperforms the 120°-configuration in angle accuracy, which is as expected. While Fig. 10 shows a difference in angle accuracy of at most one millidegree, converting to distance at the range of 15 km, which was used for the vehicle ranges in the simulations, yields about one quarter of a meter. As time increases, the estimates will converge to their true values as shown in Section VIII; hence, the largest differences in performance of different configurations are realized near $t = 0$.

The FIM can also be used as a partial check on our results for J_β and The Angle Rule. First, we make a change of coordinates

from (x_O, y_O) to (ρ, β) with the middle vehicle as the origin. Using (25) with

$$x_O = x_2 + \rho\cos\beta$$
$$y_O = y_2 + \rho\sin\beta$$

we take $(\partial h/\partial\rho)$ and $(\partial h/\partial\beta)$ to get a new measurement matrix based on polar coordinates, call it $\bar{C}$, which has the following components (superscript $*$ indicates that the variable is based on the nominal/true radar position):

$$\begin{aligned}
\bar{c}_{11} &= -\cos\beta^*\cos\theta^*_{1O} - \sin\beta^*\sin\theta^*_{1O} - 1\\
\bar{c}_{21} &= -\cos\beta^*\cos\theta^*_{3O} - \sin\beta^*\sin\theta^*_{3O} - 1\\
\bar{c}_{12} &= \rho^*(\sin\beta^*\cos\theta^*_{1O} - \cos\beta^*\sin\theta^*_{1O})\\
\bar{c}_{22} &= \rho^*(\sin\beta^*\cos\theta^*_{3O} - \cos\beta^*\sin\theta^*_{3O}) \qquad (22).
\end{aligned}$$

Taking $\det(\bar{C}^{\mathrm{T}}\bar{C})$ as our information function would just give the same result as in (21). To focus on accuracy of the angle coordinate β and exclude consideration of ρ, we must examine the component of the FIM that involves only the sensitivity of β, which is $\bar{M}_{22}$. Putting $\bar{C}$ from (22) into (20) and converting again to the separation angles $\bar{\theta}_1, \bar{\theta}_3$, we get the bottom right component

$$\bar{M}_{22} = \bar{c}_{12}^2 + \bar{c}_{22}^2 = \sin^2\bar{\theta}_1 + \sin^2\bar{\theta}_3 \qquad (23)$$

where $\rho^* = 1$ and $\beta^* = 2\pi - \theta_{2O} = 270^\circ$ for scaling and orientation, respectively. In keeping with the domain, direction, and ordering for $\bar{\theta}_1$ and $\bar{\theta}_3$, $\bar{M}_{22}$ has maxima at $\bar{\theta}_1 = 90^\circ, \bar{\theta}_3 = 90^\circ$; $\bar{\theta}_1 = 90^\circ, \bar{\theta}_3 = 270^\circ$; and $\bar{\theta}_1 = 270^\circ, \bar{\theta}_3 = 90^\circ$. Thus, the FIM tells us where maximum information gain will be achieved, which agrees with our results, but it does not give an optimal configuration for actually constructing an estimate of β, which our results *do* provide through J_β in (17). In fact, two of the three configurations suggested by maximizing (23) would render the middle radar unobservable since ECAVs 1 and 3 would be in the same location.

VI. Linearized Estimation Model

To formally minimize the variance of the middle radar position estimates apart from choosing ECAV trajectories, a nonlinear model is formulated and then linearized about the nominal state trajectory—that is, the best guess for the radar position. An Extended Kalman Filter can then be applied to the linearized model. We start with a simple model

$$\dot{q} = \begin{bmatrix}\dot{x}_O\\ \dot{y}_O\end{bmatrix} = \begin{bmatrix}0\\0\end{bmatrix} =: f(q,t) \qquad (24)$$

$$z = \begin{bmatrix}d_1 - d_2\\ d_3 - d_2\end{bmatrix} + \begin{bmatrix}n_1\\ n_2\end{bmatrix} =: h(q,t) + \frac{\mathrm{d}e}{\mathrm{d}t},$$
$$d_i(t) = \sqrt{[x_i(t) - x_O]^2 + [y_i(t) - y_O]^2} \qquad (25)$$

where $q := (x_O, y_O)$ is the true position of the middle radar, z contains the TDOA measurements (5), e is a Wiener process with zero mean and incremental covariance $R_e\mathrm{d}t$, and (x_i, y_i) is the position of ECAV i from (1) and (2). Linearizing around q^* gives

$$\delta\dot{q} = A(t)\delta q \qquad (26)$$
$$\delta z = C(t)\delta q + \frac{\mathrm{d}e}{\mathrm{d}t} \qquad (27)$$

where $\delta q := q - q^*$ and $\delta z := z - h(q^*, t)$, and the Jacobians $(\partial f/\partial q)$ and $(\partial h/\partial q)$ are evaluated at the nominal trajectory q^* to get $A(t)$ and $C(t)$, respectively. The Jacobian $(\partial f/\partial u)$ used to get $B(t)$ is undefined because the radar is assumed stationary with no control inputs for now. The system matrices are

$$A(t) = 0 \qquad (28)$$
$$C(t) = \begin{bmatrix}\cos\theta^*_{2O} - \cos\theta^*_{1O} & \sin\theta^*_{2O} - \sin\theta^*_{1O}\\ \cos\theta^*_{2O} - \cos\theta^*_{3O} & \sin\theta^*_{2O} - \sin\theta^*_{3O}\end{bmatrix} \qquad (29)$$

where θ^*_{iO} is the bearing of ECAV i from the nominal radar position. Observe that to obtain C, ECAV 2 needs only to know the bearings of ECAVs 1 and 3 from the nominal position of the middle radar; this further confirms the result in Section V that the distances of ECAVs 1 and 3 do not affect the first-order sensitivity of the estimate to measurement noise.

Since A has zero rank, the observability of (A, C) depends only on the rank of C. Taking its determinant

$$\begin{aligned}
\det C = {}& \cos\theta^*_{1O}(\sin\theta^*_{3O} - \sin\theta^*_{2O})\\
&+ \cos\theta^*_{2O}(\sin\theta^*_{1O} - \sin\theta^*_{3O})\\
&+ \cos\theta^*_{3O}(\sin\theta^*_{2O} - \sin\theta^*_{1O}) \qquad (30)
\end{aligned}$$

we see that $\det C \neq 0$ or C has full rank provided none of the three angles are equal. Thus, (A, C) is observable when all ECAVs have different bearings from the middle radar.

One might wonder why we are building a dynamical system for filtering when the current problem is really just parameter estimation, which is solvable using C with a least squares approach. We are keeping a more general structure for two specific reasons: 1) to accommodate possible motion models for the radar and 2) to provide a general structure allowing some of the ECAV states to also be estimated.

VII. Minimum Variance Estimation Theory

A. Kalman Filter

Given a general linear system model in the form of a stochastic differential equation (see [12] and [14] for theory)

$$\mathrm{d}x = A(t)x\mathrm{d}t + B(t)u\mathrm{d}t + \mathrm{d}v$$
$$y\mathrm{d}t = C(t)x\mathrm{d}t + \mathrm{d}e$$

where v and e are independent Wiener processes with zero mean and incremental covariances $R_v\mathrm{d}t$ and $R_e\mathrm{d}t$, the observer and its error are given by

$$\mathrm{d}\hat{x} = A\hat{x}\mathrm{d}t + Bu\mathrm{d}t + K[y\mathrm{d}t - C\hat{x}\mathrm{d}t] \qquad (31)$$
$$\mathrm{d}\tilde{x} = [A - KC]\tilde{x}\mathrm{d}t + \mathrm{d}v + K\mathrm{d}e \qquad (32)$$

where $K(t)$ is the observer gain, $\hat{x}$ is the state estimate, and $\tilde{x} := x - \hat{x}$ is the error. Note that $x = \delta q$ and $y = \delta z$ for our linearized system. To find the gain that minimizes the variance of the estimates, define the state covariance matrix $P(t) := \mathrm{E}(\tilde{x}\tilde{x}^{\mathrm{T}})$. Using (32) and completion of squares, the time evolution of P can be written as

$$\frac{\mathrm{d}P}{\mathrm{d}t} = \left[K - PC^{\mathrm{T}}R_e^{-1}\right] R_e \left[K - PC^{\mathrm{T}}R_e^{-1}\right] + AP + PA^{\mathrm{T}} + R_v - PC^{\mathrm{T}}R_e^{-1}CP.$$

K is then selected to make the first part of this equation zero, which gives K based on the solution to a Differential Riccati equation for P

$$K = PC^{\mathrm{T}}R_e^{-1}, \tag{33}$$

$$\frac{\mathrm{d}P}{\mathrm{d}t} = AP + PA^{\mathrm{T}} + R_v - PC^{\mathrm{T}}R_e^{-1}CP \tag{34}$$

$$P(0) = P_0.$$

Note that all the system matrices are in general time-dependent. The time-varying Kalman Filter (31)–(34) can be shown to converge under certain reasonable conditions [15]. Its drawback when operating on *linearized* systems is that the system matrices depend on the nominal state trajectory, which is often the *initial* estimate.

B. Extended Kalman Filter

Conversely, the Extended Kalman Filter (EKF) that we use updates the linearized matrices with the *current* estimate whenever a new measurement is taken. That is, at the jth time step we use the current value of $\delta\hat{q}$ to make the updates (notation from the previous section is being used here)

$$q^*_{j+1} = q^*_j + \delta\hat{q}$$

$$A_{j+1} = \left.\frac{\partial f}{\partial q}\right|_{q^*_{j+1}}$$

$$C_{j+1} = \left.\frac{\partial h}{\partial q}\right|_{q^*_{j+1}}$$

and then reset $\delta\hat{q} = 0$ and run the Kalman Filter (31)–(34) for $j+1$. Although the EKF performs better on average, its global convergence cannot be proven in general, and in adverse cases it can actually diverge.[7]

C. How the FIM is Connected to the Kalman Filter

Since the Kalman Filter really incorporates all measurements from $t = 0$ to the present, we define a new Fisher Information Matrix Q that depends on measurements over this entire interval instead of just at an instant of time as defined in Section V-B. Since the Kalman Filter is an efficient estimator for a linear system, it achieves equality of (19) implying that

$$Q = P^{-1}.$$

[7]Local convergence of the EKF has been proven for a time-invariant system; similar results are expected for time-varying systems [16].

Differentiating Q with respect to time and using (34), get

$$\frac{\mathrm{d}Q}{\mathrm{d}t} = -P^{-1}\frac{\mathrm{d}P}{\mathrm{d}t}P^{-1} = -QA - A^{\mathrm{T}}Q - QR_vQ + C^{\mathrm{T}}R_e^{-1}C$$

which provides an alternative update for the Kalman Filter also known as the Information Filter. With no dynamics, A and R_v are zero, and substituting in (20) gives

$$\frac{\mathrm{d}Q}{\mathrm{d}t} = M \tag{35}$$

which shows that the old FIM $M(t)$ based on measurements only at time t is just the rate of the new FIM $Q(t)$.

Reverting back to the old FIM (20) and again setting A and R_v to zero, (32) and (34) can be rewritten as

$$\mathrm{d}\tilde{x} = -PM\tilde{x}\mathrm{d}t + K\mathrm{d}e \tag{36}$$

$$\frac{\mathrm{d}P}{\mathrm{d}t} = -PMP. \tag{37}$$

Thus, we see from (37) that M is the Hessian of $-(\mathrm{d}P/\mathrm{d}t)$ when there are no system dynamics; it determines how fast the covariance of the estimates decreases with time. Moreover, (36) shows that the estimation error decreases based on the gain PM. Both components are crucial—M quantifies how much information is being extracted from the measurements at each instant in time or how accurate the measurements are expected to be, and P describes the covariance of the estimates over time or how much they should be trusted as opposed to the measurements. This concept may be helpful as a guide for improving the first estimation method in Section IV-A.

VIII. EKF Application to the Linearized Model

We now apply the theory from Section VII to the model in Section VI to estimate the middle radar position over time in a scenario with a fixed phantom track. The reason we choose to use an EKF instead of just a Kalman Filter is so that $C(t)$ in (29) can be updated based on the current estimate of the radar position. The increase in performance becomes noticeable when the initial estimate is poor.

A. Analysis of the Filtered System

In our case, we can prove that the variance of the estimates converges to zero, *even when using an EKF*. First, rewrite (34) using (28), $R_v = 0$, and $R_e = \mathrm{diag}(R_{ei}, R_{ei})$

$$\dot{P} = -\frac{1}{R_{ei}}PC^{\mathrm{T}}CP. \tag{38}$$

Because the ECAVs are generating a phantom track, their bearings from the middle radar will be different at any given time, so $\det C \neq 0$ as discussed before using (30). With the invertibility of $C(t)$ established for all t, set $\dot{P} = 0$ in (38) and get

$$0 = PC^{\mathrm{T}}CP = (CP)^{\mathrm{T}}(CP) \Leftrightarrow CP = 0 \Leftrightarrow P = 0$$

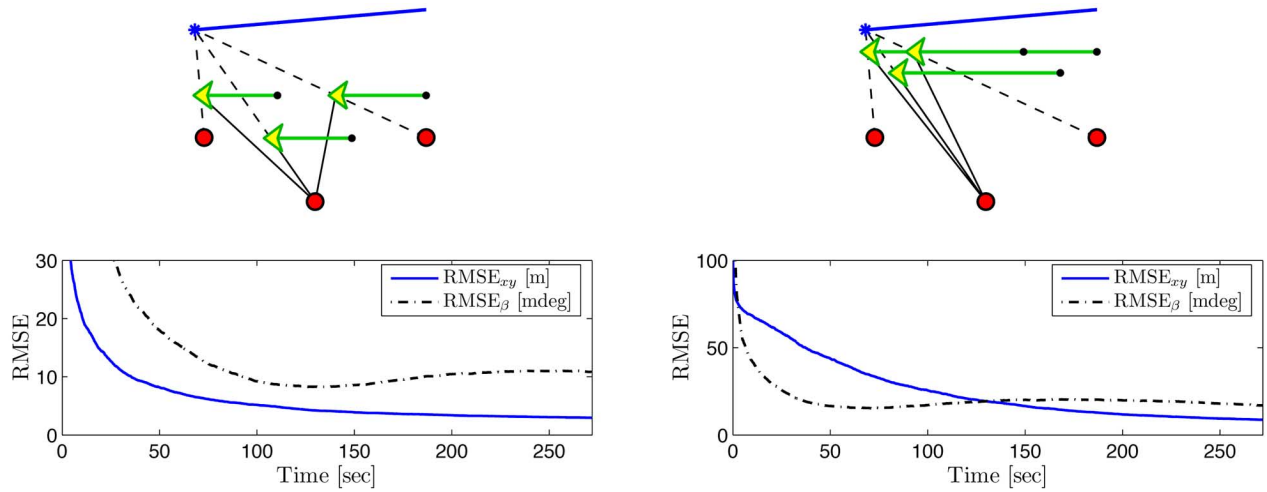

(a) for $\frac{r_0}{R_0} = 0.33$ (b) for $\frac{r_0}{R_0} = 0.67$

Fig. 11. Estimation of the middle radar position using an EKF. An EKF is applied to the linearized system; the measurement noise has intensity 0.0001 km^2/Hz, and 1000 runs are made. The root mean square errors of the position and angle estimates are plotted as RMSE$_{xy}$ and RMSE$_{\beta}$, respectively. The only difference between the two scenarios is how far the vehicles are from the radars, which affects their relative separation angles and hence the errors.

which shows that 0 is the unique equilibrium for P. Second, it can be shown starting with (38) that

$$\begin{aligned}\dot{p}_{11} &= \left(c_{11}^2 + c_{21}^2\right) p_{11}^2 + \left(c_{12}^2 + c_{22}^2\right) p_{12}^2 \\ &\quad + 2(c_{11}c_{12} + c_{21}c_{22}) p_{11} p_{12} \\ \dot{p}_{22} &= \left(c_{11}^2 + c_{21}^2\right) p_{12}^2 + \left(c_{12}^2 + c_{22}^2\right) p_{22}^2 \\ &\quad + 2(c_{11}c_{12} + c_{21}c_{22}) p_{12} p_{22}\end{aligned}$$

are nonpositive by using the identity $x^2 + y^2 \geq 2xy$ twice for each equation, which means that $p_{11}(t)$ and $p_{22}(t)$ are monotonically nonincreasing for any C. Also, by definition p_{11} and p_{22} are bounded below by zero. Therefore, $\lim p_{11}$ and $\lim p_{22}$ exist and must equal 0.

Steady-state will not be reached in practice since the deception process occurs in a short time. It is therefore desirable that the variance of the position estimates decrease as rapidly as possible over this interval, which is governed by the FIM as already discussed.

B. Simulations of Estimation by Filtering

Both scenarios here are identical to those in Fig. 6. Fig. 11 shows the results of position estimation by applying an EKF to the linearized system (26)–(29). The state covariance is initialized as $P_0 = \mathrm{diag}((1/2)\sigma_O^2, (1/2)\sigma_O^2)$, where $\sigma_O = 100$ m is the standard deviation of the initial guess from the true radar position. For each run, the x and y components of the initial guess are chosen randomly with a standard deviation of $(1/\sqrt{2})\sigma_O$, and the measurement noise sequences are also chosen randomly. As in the earlier simulations, the errors for both the coordinate and the angle estimates are plotted using (11) and (12), respectively.

C. Comparison With the First Method

We refer here to the first method, which is direct calculation using (9)–(10) and then time averaging, and the second method, which is the EKF applied to the linearized system (26)–(29). Comparing Fig. 11 with Fig. 6, the performance of the second method is overall an improvement. Fig. 11(a) shows that when the ECAVs are close to the radars, the second method performs similar to the first. As the ECAVs move further from the radars, Fig. 11(b) shows that the second method has error lower than the first by more than an order of magnitude, and it does not increase with time. As shown earlier, the variance of the estimates from the second method converges to zero, but only as time goes to infinity. In summary, the EKF provides better performance than direct calculation with time averaging, as currently designed. In particular, the EKF provides lower error when the information is poor.

In addition to the communication needed for the TDOAs, the first method requires ECAV 2 to know the relative ranges and angles of ECAVs 1 and 3. The second method requires ECAV 2 to know the positions of ECAVs 1 and 3 since $h(q^*, t)$ in (25) must be determined for the EKF, so nothing is gained in terms of more or less information required. However, the second method depends on the initial estimate whereas the first does not. The first method uses two TDOAs to get a closed form solution; if additional TDOAs are used, the corresponding solutions—one for each set of two TDOAs—must somehow be combined. The second method requires at least two TDOAs, but can easily fuse additional measurements to improve accuracy. The first method allows direct calculation of the *angle* estimate for the radar, which is the only part of the position estimate for which high accuracy is needed to minimize the variance of the phantom track. The second method provides the estimate in *coordinate* components, which are unnecessary, and so working with a direct limit on the accuracy of the angle estimate would be more difficult. However, the initialization for P_0 in the EKF could be chosen to cause one of the coordinates to converge faster to its true value, which could help improve the accuracy of the angle estimate. The first method is simpler computationally, but both methods are quite feasible with modern technology.

IX. Conclusion

Position estimation using TDOA techniques was explored. An explicit solution was developed for the middle radar position in polar coordinates using two TDOA measurements. Using this result, estimation by direct calculation and time averaging gives reasonable results as shown by simulation. The simulations also show that performance is drastically affected by the trajectories the ECAVs fly. Starting with the explicit solution for the radar position, the sensitivity of the estimate due to measurement noise was calculated and analyzed. The main results are that this sensitivity depends critically on the separation angles between vehicles and does not depend up to first order on their distances from the radar. The analysis culminates in The Angle Rule: for three vehicles, one of which is the reference, the optimal configuration for the angle estimate is 90° separation between the reference and the other vehicles. Calculating the Fisher Information Matrix based on the radar position coordinates leads to The Coordinate Rule: for three vehicles, the optimal configuration for the position estimate is 120° separation.

A simple linearized model was developed using the TDOA measurements as outputs. An EKF applied to this system yields overall improvement as compared by simulation to the earlier estimation scheme. Analysis of the filtered system shows that the variance of its estimates converges to zero with time. Also, there is a nice connection between the Kalman Filter and the Fisher Information Matrix, which actually determines how fast the covariance of the state estimate decreases.

The smart integration of more than two TDOA measurements should increase the estimation accuracy for the first method and should be investigated; with a closed-form solution no longer known, other techniques might prove useful such as nonlinear least squares. Performance of the first method may be further improved by updating the estimate based on its covariance and the information gain of the measurements. Also, other realistic sources of error in generating the phantom track, such as wind disturbances and inaccurate ECAV positions, could be included in the system model.

References

[1] K. B. Purvis, P. R. Chandler, and M. Pachter, "Feasible flight paths for cooperative generation of a phantom radar track," *AIAA J. Guidance, Control, Dynamics*, vol. 29, no. 3, pp. 653–661, May–Jun. 2006.

[2] M. Pachter, P. R. Chandler, R. A. Larson, and K. B. Purvis, "Concepts for generating coherent radar phantom tracks using cooperating vehicles," in *Proc. AIAA Conf. Guidance, Navigation, Control*, Providence, RI, Aug. 2004, paper no. AIAA-2004–5334.

[3] R. G. Brown and P. Y. Hwang, *Introduction to Random Signals and Applied Kalman Filtering*, 3rd ed. New York: Wiley, 1997.

[4] K. B. Purvis, K. J. Åström, and M. Khammash, "Estimating radar positions using cooperative unmanned air vehicle teams," in *Proc. Amer. Control Conf.*, Portland, OR, Jun. 2005, vol. 5, pp. 3512–3517.

[5] T. Shima, P. R. Chandler, and M. Pachter, "Decentralized estimation for cooperative phantom track generation," in *Proc. 5th Int. Conf. Cooperative Control Optimiz.*, River Edge, NJ, Jan. 2005, World Scientific.

[6] K. B. Purvis, K. J. Åström, and M. Khammash, "Online control strategies for highly coupled cooperative UAVs," in *Proc. Ameri. Control Conf.*, New York, Jul. 2007, pp. 3961–3966.

[7] F. Gustafsson and F. Gunnarsson, "Positioning using time-difference of arrival measurements," in *Proc. IEEE Int. Conf. Acoust., Speech, Signal Process.*, Apr. 2003, vol. 6, pp. 553–556.

[8] F. Gustafsson and F. Gunnarsson, "Mobile positioning using wireless networks: Possibilities and fundamental limitations based on available wireless network measurements," *IEEE Signal Process. Mag.*, vol. 22, no. 4, pp. 41–53, Jul. 2005.

[9] M. Aatique, "Evaluation of TDOA Techniques for Position Location in cdma Systems," M.S. thesis, Virginia Polytechnic Inst. and State Univ., Blacksburg, 1997.

[10] K. B. Purvis and P. R. Chandler, "A review of recent algorithms and a new and improved cooperative control design for generating a phantom track," in *Proc. Amer. Control Conf.*, New York, Jul. 2007, pp. 3252–3258.

[11] S. Martínez and F. Bullo, "Optimal sensor placement and motion coordination for target tracking," *Automatica*, vol. 42, no. 4, pp. 661–668, 2006.

[12] Y. Bar-Shalom, X.-R. Li, and T. Kirubarajan, *Estimation with Applications to Tracking and Navigation*. New York: Wiley, 2001.

[13] D. Uciński, *Optimal Measurement Methods for Distributed Parameter System Identification*. Boca Raton, FL: CRC, 2005.

[14] K. J. Åström, *Introduction to Stochastic Control Theory*. New York: Academic, 1970.

[15] T. Kailath, A. H. Sayed, and B. Hassibi, *Linear Estimation*. New York: Prentice-Hall, 2000.

[16] A. J. Krener, , A. Rantzer and C. Byrnes, Eds., "The convergence of the extended kalman filter," in *Directions in Mathematical Systems Theory and Optimization*. Berlin, Germany: Springer-Verlag, 2002, pp. 173–182.

Keith B. Purvis (M'07) received the B.S. degree in mechanical engineering from the University of Idaho, Moscow, in 2002 and the M.S. and Ph.D. degrees from the University of California, Santa Barbara, in 2004 and 2007, respectively.

His research interests are in the area of cooperative control and estimation for multiple agents. In cooperative control, he has developed strategies based on optimal control and also decentralized control to address the issues of strong coupling, uncertainty, and partial information. In estimation, he has designed and applied Kalman filters and has used novel parameterizations of the estimate as well as information theory to determine optimal sensor/platform configurations. His research has been in close collaboration with the Air Force Research Laboratory, including two summers spent onsite at Wright–Patterson AFB. He is a certified private pilot and was a U.S. Air Force Academy Appointee in 1997.

Karl J. Åström (F'96) is Emeritus at Lund University, Lund, Sweden, and a Visiting Professor at the Department of Mechanical Engineering, University of California, Santa Barbara. He has broad interests in control theory and its applications.

Prof. Åström, who has Erdös number 3, is a Fellow of the IFAC. He has received many honors—among them the 1987 Quazza Medal from IFAC and the 1993 Medal of Honor from the IEEE.

Mustafa Khammash (F'07) received the B.S. degree from Texas A&M University, College Station, in 1986 and the Ph.D. degree from Rice University, Houston, TX, in 1990, both in electrical engineering.

He is the Director of the Center for Control, Dynamical Systems, and Computations (CCDC), University of California, Santa Barbara (UCSB). He also holds a Professor appointment in Mechanical Engineering, UCSB. In 1990, he joined the Electrical Engineering Department at Iowa State University (ISU), Ames. While at ISU, he created the dynamics and control program and led that control group until 2002, when he joined the dynamics and control group in the Department of Mechanical and Environmental Engineering at UCSB. His research interests are in the area of control theory and its applications to engineering and to biological systems.

Prof. Khammash is the recipient of the National Science Foundation Young Investigator Award, the Japan Society for the Promotion of Science (JSPS) Fellowship, the ISU Foundation Early Achievement in Research and Scholarship Award, the ISU College of Engineering Young Faculty Research Award, and the Ralph Budd Best Engineering Ph.D. Thesis Award.